Energetics of Exciton Binding and Dissociation in Polythiophenes: A Tight Binding Approach

Journal:	*Physical Chemistry Chemical Physics*
Manuscript ID	CP-ART-02-2019-001116.R1
Article Type:	Paper
Date Submitted by the Author:	13-May-2019
Complete List of Authors:	Bombile, Joel; Pennsylvania State University, Chemical Engineering Janik, Michael; Pennsylvania State University, Chemical Engineering Milner, Scott T. ; Penn State University,

Journal Name

Energetics of Exciton Binding and Dissociation in Polythiophenes: A Tight Binding Approach

Joel H. Bombile, Michael J. Janik, and Scott T. Milner*

Organic photovoltaics offer a potential low-cost alternative to inorganic solar cells. Crucial to the performance of these devices is the generation of free charges, which occurs through the dissociation of excitons. Here we study excitons in polythiophenes, their stability and energetics of dissociation and separation into charge carriers. Excitons are excited electron and hole pairs bound by Coulomb interactions. To separate into unbound charges, the exciton binding energy must be overcome. We use a tight binding Hamiltonian to describe the exciton binding energy and its dissociation potential, for an exciton confined to a single polymer chain. Our model accounts for polaronic effects, arising from reorganization of nuclei and from polarization of the surrounding dielectric, which stabilize the separated carriers and thereby affect the exciton dissociation potential. We examine the effects of an applied electric field on the dissociation potential, and relate the field strength necessary to unbind the hole-electron pair to the maximum attractive Coulomb force between them. We apply our model to study the exciton at a donor-acceptor interface on a block-copolymer. Interfacial polarization alters the exciton binding potential, rendering the hole-electron pair easier to unbind.

Introduction

Semiconducting polymers are the subject of much interest and study as active elements in a number of electronic devices, including light emitting diodes[1], field effect transistors[2], and photovoltaic cells[3]. Among these devices, organic photovoltaics (OPV) are particularly attractive as a low cost alternative photovoltaic technology due to their light weight, flexibility, thin film character, ease of manufacturing by printing techniques even on flexible substrates, and production from abundant and non-toxic materials. These unique characteristics are set to enable applications that are difficult to realize with traditional inorganic materials[4–6].

Crucial to the performance of photovoltaic devices is the generation of free charge carriers, which occurs through the dissociation of excitons. Excitons are excited electron and hole pairs bound by Coulomb interactions. In photovoltaic devices, singlet excitons form when light is absorbed in the active layer, made of a photo-responsive semiconductor. For separation into individual charge carriers, the electron-hole binding energy must be overcome. In inorganic solar cells, excitons are weakly bound and readily dissociate to form free carriers under thermal energy[6]. In contrast, excitons in OPVs are tightly bound. Their dissociation relies on a two-component system made of an electron donor

and an electron acceptor material, typically in a bulk heterojunction (BHJ) structure. Exciton dissociation occurs at the donor-acceptor interface, where the electron is transferred to the acceptor, driven by the difference in electron affinity between the two materials[6]. Because of the strong Coulomb interaction between the hole and the electron, they remain bound even though they now reside on two different materials across the donor-acceptor interface. Complete dissociation or charge separation is driven by an external electric field, or induced by quenched structural disorder within the semiconductors[7]. If the exciton is not able to dissociate within its lifetime, it will undergo recombination back to the ground state, resulting in the loss of the energy gained from photon absorption[6]. A clear understanding of exciton formation, dissociation, and recombination in OPVs is necessary for the design of more efficient devices.

We focus on the stability of excitons in organic semiconducting polymers, and the energetics of their dissociation and separation into charge carriers, which can then be transported to the electrodes. The stability of an exciton is measured by its binding energy, which quantifies the energy needed to separate this exciton into free hole- and electron-polarons. For singlet excitons, the exciton binding energy is practically evaluated as the energy difference between the transport gap and the excitation energy to the lowest lying dipole-allowed singlet excited state[8–10]. The exciton binding energy of organic semiconductors is in the range of 0.5 - 1 eV[4,5,7], and is still debated due to difficulties in deter-

* corresponding author

Pennsylvania State University, University Park, PA 16802, USA. Fax: +1 (814) 865-7846; Tel: +1 (814) 863-9355; E-mail: stm9@psu.edu

mining it experimentally or computationally.

From an experimental point of view, one must accurately measure the optical gap (which gives the excitation energy) and the transport gap. The optical gap is measured by optical absorption, while the transport gap is estimated from a combination of ultraviolet photoelectron spectroscopy (UPS) and inverse photoemission spectroscopy (IPES) [8,10]. Computationally, the binding energy is determined by evaluating the same two quantities, for which various *ab*-initio and semi-empirical methods have been used.

Among the first-principles methods, the state-of-the-art is many-body perturbation theory using the *GW* approximation and the Bethe-Salpeter equations (BSE), shown to provide reliable quantitative predictions of excited states for organic systems [11–26], including the optical gap and the transport gap. However this method shows some reliance on the mean-field starting point used in the perturbative approach, and comes at a large computational cost [25,26], making it impractical to be applied to large systems.

The other commonly used *ab*-initio method is time-dependent density functonal theory (TDDFT). Though widely applied to predict the excited state properties of molecules, TDDFT shows significant dependance on the exchange-correlation (XC) functional, with the most used functionals (PBE [27], a semilocal functional, and B3LYP [28–30], a global hybrid functional) recently shown to severely fail at predicting the transport gap [9] and some excited state properties such as charge-transfer excitation energies for organic semiconductors [31–33]. The failure of these functionals can be attributed to the self-interaction error [33–35], which results in too much localization or delocalization of molecular orbitals, described in details elsewhere [36,37]. Recent efforts in reducing the self-interaction error, and its implication in the description of several properties, has led to the development of non-empirically tuned range-separated hybrid functionals [38–41]. The use of these functionals has shown remarkable success in describing ground and excited state properties relevant in organic electronic materials research [31,42–46], including singlet exciton binding energies [9]. Although much less expensive than the GW-BSE approach, TDDFT with range-corrected functionals still presents limitations in the system sizes to which it can be practically applied. Here we note that the issue of computational cost of this method has been recently addressed with the simplified Time-Dependent Density Functional Theory (sTD-DFT) approach, with some compromise on accuracy.

Semi-empirical models offer an attractive alternative to *ab*-initio techniques. Being much less computationally expensive, these methods allow access to much larger system sizes, and have been widely applied to study of the dynamics of excited states in organic semiconductors. In particular for excitons in conjugated polymers, the commonly used methods are the Su-Schrieffer-Heeger (SSH) model [47–51], often used in an extended form including the Hubbard [52] electron-electron interaction effects, and the Pariser-Parr-Pople (P-P-P) model [53–56]. Both these models are quantum-based approaches employing the tight-binding formalism. They have proved useful in providing qualitative understanding of excited state static and dynamic properties; quanti-

tative accuracy can also be achieved with careful parametrization [54].

Here we use a similar model Hamiltonian to describe the binding energy and dissociation potential (i.e., energy versus relative position of electron and hole), for a singlet exciton confined to a single polymer chain. The main objective of the model is to describe qualitatively and quantitatively the dissociation/binding potential of the exciton, so as to elucidate how factors such as an electric field or a donor-acceptor interface affect the energetics of the hole-electron pair. Establishing such potential requires a reliable description of the continuum between the bound exciton and the separated/free hole and electron polarons, which will be difficult to accomplish with available first-principles methods.

As in the P-P-P model, we adopt a quantum description of the electron, the hole and their Coulomb interaction, following the tight-binding approximation. Our model takes into account polaronic effects arising from the reorganization of nuclei and from polarization of the surrounding dielectric, handled classically as described in our previous work [57]. These effects substantially stabilize the separated carriers and affect the exciton dissociation potential. We apply our model to poly(3-hexylthiophene) (P3HT), chosen as a model polymer. All parameters besides the exciton Coulomb interaction are adopted from our previous work [57,58], where they were determined by periodic DFT calculations. The Coulomb interaction parameter is determined by TDDFT calculations, using a non-empirically tuned range-corrected functional.

We examine the effect of an applied electric field on the exciton binding potential. We want to know how the exciton is polarized by the field, and determine how large a field would be needed to unbind the electron-hole pair, i.e., overcome their Coulomb attraction, in the absence of any other factors, such as an interface or energetic disorder. Then we consider the exciton at a covalent donor-acceptor interface along a block copolymer. The LUMO energy offset at the interface polarizes the exciton. We quantify the induced hole-electron separation and observe how the exciton dissociation potential is altered by the interface.

Our transparent and flexible tight binding model, with carefully determined parameters, provides qualitative and quantitative description of the continuum between the bound exciton and the free electron and hole polarons after dissociation. In addition, the model shows the contribution of polarization of the surrounding environment and nuclei reorganization on the energetics of exciton binding/dissociation. Although not included in this work, the model is well suited to studying the effects of energetic and spatial disorder, which are known to play an important role in the generation of free charge carriers from exciton dissociation [59,60].

The rest of the paper is organized as follows. We begin by presenting the tight-binding model used to describe the electron and hole on a polymer chain. We detail the components that dictate the exciton energy within our model: the kinetic energy of the electron and hole, their onsite Coulomb interaction energy along with the TD-DFT determination of this relevant parameter, and the stabilization energy arising from the polarization of the surrounding dielectric medium and the reorganization of nuclei. Then, we show our calculated optimal singlet exciton for P3HT for two cases: (1) "vertical" exciton on an isolated chain,

(2) exciton in a polarizable medium with nuclei reorganization. Comparison is made to GW-BSE and TD-DFT results to validate our TB model. We then compute the exciton dissociation potential (i.e., energy versus hole-electron distance) and discuss how it changes with the dielectric constant of the medium. Finally we present the exciton dissociation by an external electric field and by a donor-acceptor 1D interface with a given HOMO and LUMO energy offset.

Tight-binding Hamiltonian

We describe a charge carrier (electron or hole) on a polymer chain using the tight-binding model, as in our previous work[57,58]. Following this model, the electron or the hole occupies sites with some onsite energy, and is stabilized by hopping between neighboring sites, with hopping restricted to immediate neighbors. The polymer chain is modeled as a one-dimensional array of sites, each site corresponding to a monomer unit or moiety along the polymer backbone. For P3HT, a thiophene ring constitutes a site. The Hamiltonian is

$$H = \sum_k \varepsilon_k c_k^\dagger c_k - \sum_k t_k (c_k^\dagger c_{k+1} + c_{k+1}^\dagger c_k) \quad (1)$$

Here $c_k^\dagger$ and c_k are creation and annihilation operators for an electron on site k; ε_k is the onsite energy of the carrier at site k; and t_k is the hopping matrix element between sites k and $k+1$.

The electron and hole are two different particles and therefore have different ε and t_k values, determined by ground-state DFT calculations. The onsite energies are determined from the energy of the HOMO (for a hole) and LUMO (for an electron) of the moiety making up a site. The onsite energies govern the HOMO and LUMO energy levels for the overall polymer chain. These values will be varied on either side of a covalent donor-acceptor interface in Section 6, when we study the effects of interfacial energy level offset on exciton dissociation. The hopping matrix elements for the hole and electron were obtained from the widths of valence and conduction bands for the polymer chain[58].

Exciton binding energy

We want to define the exciton binding energy in a simple and tractable manner. As such, we choose the HOMO - LUMO gap, i.e., the energy difference between the extended states of the hole and electron in an infinitely long polymer chain, as a reference. This is illustrated in Figure 1, which shows the gap energy levels for the polymer for three cases: (i) in the ground state (gap, $E_{LUMO} - E_{HOMO}$), (ii) during charge transport (transport gap, $P^- - P^+$, with P^- and P^+ being negative and positive polaron energy levels,) and (iii) after singlet exciton formation (optical gap, $S_1 - S_0$, in the bound exciton)[8]. Below, we reference the exciton binding energy to the band gap; note that we do not explicitly compute the band gap itself.

The terms entering the exciton energy are: (1) the kinetic energy of the two carriers, (2) the Coulomb interaction between the two charge carriers, (3) the stabilization energy from polarization of the surrounding dielectric medium (polarization energy), and (4) the stabilization energy from reorganization of coupled nuclei (reorganization energy). Below we describe each of these
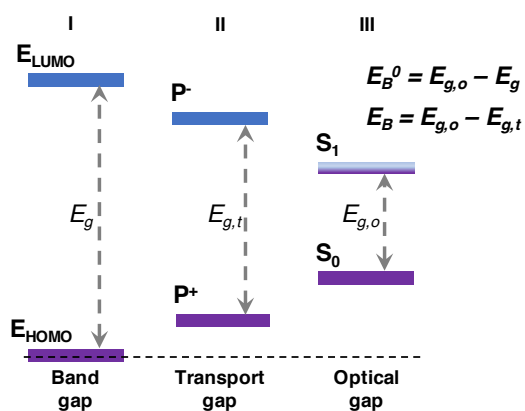
Fig. 1 HOMO - LUMO gap and gap energy levels for a polymer chain in the ground state (I), during charge transport (II), and after photoexcitation (III). (adapted from Deibel *et al*[8].)

energy terms in detail. The description is in reference to the fully delocalized exciton in a infinitely long polymer chain. The energy of this state relative to the ground state is the band gap ($E_{LUMO} - E_{HOMO}$).

Kinetic energy of hole and electron

The kinetic energy of the hole and electron are given by the square gradient term of the electronic Hamiltonian. For the conduction electron we have:

$$\langle \psi^e | H^e | \psi^e \rangle = \varepsilon_e \sum_i |a_i^e|^2 - t_e \sum_i (a_i^{e*} a_{i+1}^e + a_{i-1}^{e*} a_k^e)$$

$$= (\varepsilon_e - 2t_e) + t_e \sum_i |a_{i+1}^e - a_i^e|^2 \quad (2)$$

Here H^e is the one-electron tight binding Hamiltonian, $|\psi^e\rangle = \sum_i a_i c_i^\dagger |0\rangle$ is the electron wavefunction, with a_i the amplitude of the wavefunction on site i, and $c_i^\dagger$ the creation operator for an electron, acting on the empty conduction band $|0\rangle$. Similarly, for the valence hole we have:

$$\langle \psi^h | H^h | \psi^h \rangle = \varepsilon_h - (\varepsilon_h \sum_i |a_i^h|^2 + |t_h| \sum_i (a_i^{h*} a_{i+1}^h + a_{i-1}^{h*} a_k^h))$$

$$= -2|t_h| + |t_h| \sum_i |a_{i+1}^h - a_i^h|^2 \quad (3)$$

where $|\psi^h\rangle = \sum_i a_i^h c_i |V\rangle$ is the hole wavefunction, with c_i the annihilation operator for an electron, acting on the full valence band $|V\rangle = \prod_i c_i^\dagger |0\rangle$. Note the sign change of the hopping term in the first line of Equation 3 in comparison to Equations 2 and 1. This is because of the asymmetry of the local thiophene HOMO orbital, in which the hole wavefunction is expanded, resulting in a negative hopping matrix element t_h[58]. The total kinetic energy of the exciton relative to the extended exciton or the band gap will be the sum of the square gradient terms for the two carriers, as given by:

$$\Delta \langle T \rangle = t_e \sum_i |a_{i+1}^e - a_i^e|^2 + |t_h| \sum_i |a_{i+1}^h - a_i^h|^2 \quad (4)$$

where we have used the fact that the extended exciton has vanishing square gradient terms in the long polymer limit. The subscripts e and h denote an electron and a hole respectively, and t has the same meaning as in Equation 1. $\Delta\langle T\rangle$ decreases with the wavefunction square gradient of both carriers, and thus favors a more extended exciton.

Electron-hole Coulomb interaction

In the absence of any reorganization of the medium surrounding the electron-hole pair, the singlet exciton energy with respect to the band gap is given by

$$\Delta\langle V\rangle_{ex} = -(V_{HLLH} - 2\delta_{ss'}V_{HLHL}) \qquad (5)$$

where s and s' are the spins of the excited electron and the electron in the singly-occupied HOMO, respectively. The two terms in the above equation are the direct and exchange Coulomb interaction between the hole and the electron. The direct term has the form

$$V_{HLLH} = \int dr dr' V(r-r')\psi^{h*}(r)\psi^{e*}(r')\psi^{e}(r')\psi^{h}(r) \qquad (6)$$

and the exchange term has the form

$$V_{HLHL} = \int dr dr' V(r-r')\psi^{h*}(r)\psi^{e*}(r')\psi^{h}(r')\psi^{e}(r) \qquad (7)$$

where $V(r) = 1/(4\pi\varepsilon_0 r)$; and $\psi^{h}(r) = \sum_i a_i^h \phi_{Hi}(r)$ and $\psi^{e}(r) = \sum_i a_i^e \phi_{Li}(r)$ are the hole and electron wavefunctions, written as a superposition of local HOMO orbital $\phi_{Hi}(r)$ and LUMO orbital $\phi_{Li}(r)$. We introduce these expansions into Equations 6 and 7. We initially have four sums over site indices in each of the two terms, but these are reduced to double sums by the fact that the orbitals $\phi_{Hi}(r)$ and $\phi_{Li}(r)$ integrated over r have to be on the same site, because they are local to each site, likewise for the orbitals integrated over r'.

$$V_{HLLH} = \sum_{i,j}|a_i^h|^2|a_j^e|^2 \int dr dr' V(r-r')\phi_{Hi}^{*}(r)\phi_{Lj}^{*}(r')\phi_{Lj}(r')\phi_{Hi}(r)$$

$$V_{HLHL} = \sum_{i,j}(a_i^{h*}a_i^e)(a_j^{e*}a_j^h) \int dr dr' V(r-r')\phi_{Hi}^{*}(r)\phi_{Lj}^{*}(r')\phi_{Hj}(r')\phi_{Li}(r)$$

$$(8)$$

The exchange integral can be shown to amount to dipole-dipole interactions between transition dipole moments located on sites i and j:

$$V_{HLHL} = \sum_{i,j}(a_i^{h*}a_i^e)(a_j^{e*}a_j^h)$$

$$\left(\frac{\mu_i \cdot \mu_j}{R_{ij}^3} - 3\frac{(\mu_i \cdot R_i)(\mu_j \cdot R_j)}{R_{ij}^5}\right) \qquad (9)$$

where $\mu = \langle\phi_H|r|\phi_L\rangle$, $R_{ij} = |R_i - R_j|$, and R_i and R_j are the position vectors of sites i and j. This result is found by observing that the dominant term of the exchange integral in Equation 8 comes from expanding $V(r-r')$ on each site about the center. The offsite

contributions to V_{HLHL} are small, because this integral scales like $1/R_{ij}^3$. We computed a contribution of less than 1 percent to the exciton binding energy. The exchange term can thus be approximated to have only an onsite contribution to the Coulomb energy. The exchange term contributes a positive amount to the exciton energy when the excited electron in the LUMO and the electron in the now-singly-occupied HOMO have the same spin (see Equation 5). As such the singlet exciton is of higher energy and more extended compared to the triplet-exciton, for which the electron and hole have opposite spins.

The direct integral can likewise be approximated as a sum of onsite and offsite contributions. These contributions have been handled in P-P-P models[54,56,61] following the Coulomb repulsion potential suggested by Ohno[62]. Here we approximate the HOMO and LUMO located on sites i and j as smeared charge distributions represented by three-dimensional Gaussians, and evaluate the integral in V_{HLLH} explicitly for offsite contributions (i.e., $i \neq j$) as $E_C(i,j)$, described in detail in Supplementary Information. The distributed charges in the HOMO and LUMO orbitals on the same site cuts off the divergence issues of the Coulomb integral when $|r-r'|$ approaches zero. We lump the onsite direct and exchange contributions into one constant V_C, and resort to TD-DFT calculations for its estimation. The hole-electron Coulomb interaction is then:

$$\Delta\langle V\rangle_{ex} = -\sum_{i,j\neq i}|a_i^h|^2|a_j^e|^2 E_C(i,j) - V_C\sum_i|a_i^h|^2|a_i^e|^2 \qquad (10)$$

Below we describe our estimation of the onsite Coulomb interaction V_C, before presenting the polarization energy.

TD-DFT calculation of V_C

To determine the onsite Coulomb interaction, we compare the prediction of Equation 10 to TD-DFT calculations for the binding energy of a singlet exciton for our system of interest. For P3HT, V_C can be estimated by TD-DFT calculations for an isolated thiophene ring, corresponding to a single site, such that $\Delta\langle V\rangle_{ex} = V_C$. We specifically compute the HOMO-LUMO gap E_g and the vertical excitation energy to the lowest lying singlet excited state, i.e., the optical gap $E_{g,o}$ without reorganization of nuclei, so that V_C is given by:

$$-V_C = \Delta\langle V\rangle_{ex} = E_{g,o} - E_g \qquad (11)$$

We perform our TD-DFT calculations in the Gaussian g09 package, using the optimally tuned long-range corrected hybrid functional LC-ωPBE* and 6-311g basis set. LC-ωPBE* uses PBE exchange-correlation in the short-range and Hartree-Fock (exact) exchange in the long-range. The ω parameter dictates the ranges of applicability of the two regimes, and is highly system-specific. We determine ω for thiophene by minimizing the difference between the negative of the HOMO energy and the vertical ionization potential[45,63]. The ring geometry was fixed to that obtained from ground state periodic DFT calculations of an infinitely long polythiophene chain, as performed in the Vienna Ab-initio Simulation Package (VASP) using the PW91[64] functional.

To illustrate the importance of the functional choice for our TD-DFT calculations, we have computed the HOMO-LUMO gap

E_g, the optical gap $E_{g,o}$ and E_B^0 for thiophene oligomers of one, two, four and seven monomers. We extrapolated these values to the infinitely-long polymer limit using a tight-binding fit, and compare the predicted limiting values to the GW-BSE data of van der Host *et al* [12]. The result for E_g and E_B^0 are shown in Figure 2.
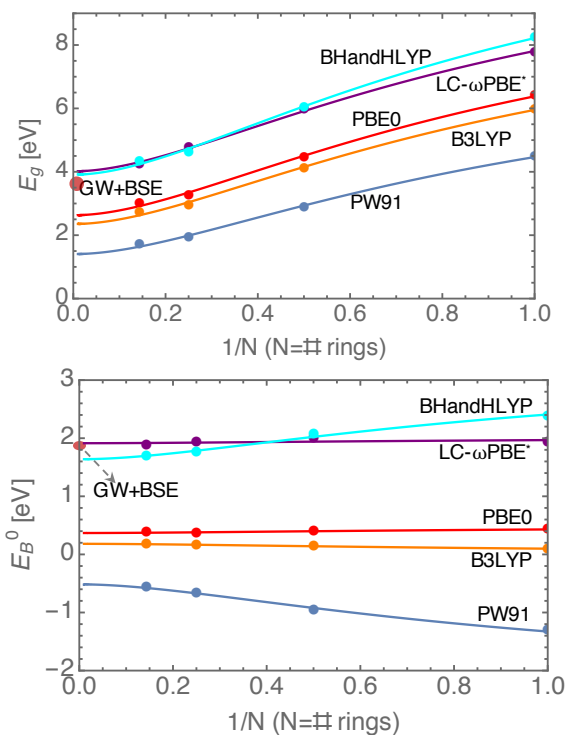
Fig. 2 HOMO - LUMO gap (a) and Singlet exciton binding energy (b) as a function of inverse chain length.

The different functionals largely disagree in their prediction of E_g (See Figure 2a,) with functionals that include more exact exchange being more accurate compared to GW-BSE. We observed a spread of only about 0.2 eV in the predicted excitation energy to the lowest singlet excited state $E_{g,o}$ between these functionals (not shown). However, the failure to predict the HOMO-LUMO gap is clearly reflected in the predicted E_B^0 values, for which LC-ωPBE* is most accurate with respect to GW-BSE, as can be seen in Figure 2b. The E_B^0 disagreement among the functionals is both qualitative and quantitative. The spread of predicted values is wider for a single monomer compared to the long-polymer limit. Note that the accuracy with which E_B^0 is predicted also affects the exciton configuration [65]. Smaller exciton sizes are associated with more tightly bound excitons and vice-versa. This highlights the importance of our choice of LC-ωPBE* for computing V_C. The result is a value of $\mathbf{V_C} = \mathbf{1.93}$ eV, obtained from $E_g = 7.78$ eV and $E_{g,o} = 5.85$ eV.

Polarization energy and electron-hole Coulomb interaction

We have discussed above the Coulomb interaction between the excited electron and the hole. Here we describe this interaction together with the interaction of the two charge carriers with the surrounding polarizable medium of dielectric constant ε_r. When the hole and electron are far apart, we should recover their re-

spective polaron states, in which the two carriers are stabilized by the surrounding polarizable medium. When the carriers are brought closer, the polarization effects decrease, since the carriers of opposite signs are competing to polarize the same surrounding (and cancel each other's charge, as they co-occupy sites along the chain.)

We treat the surrounding dielectric as a classical continuum, interacting with the net charge distributions of the two localized carrier wavefunctions. The two carrier wavefunctions are a superposition of molecular orbitals, the monomer HOMO for the hole and LUMO for the electron. The two carrier probability distributions are seen as one net charge distribution by the dielectric. As already mentioned for the offsite hole-electron Coulomb interaction above, we model the molecular orbitals crudely and conveniently as spherical Gaussians, with a radius of 2 Å, about half the size of a single thiophene ring. The net charge $q_i = q_i^h + q_i^e$ on the ith ring induces a polarization distribution $P_i(r)$ in the surrounding material. (The hole and electron onsite charges are given by $q_i^h = q_0|a_i^h|^2$ and $q_i^e = -q_0|a_i^e|^2$, with q_0 being the elementary charge.) By superposition, the total polarization distribution is the sum of the individual $P_i(r)$ terms.

The classical electrostatic energy of this system can be expressed as the sum over sites i and j of interactions: between net charges q_i and q_j, between q_i and polarization P_j, and between P_i and P_j. As for our earlier treatment of polarons, we must avoid the unphysical self-interaction of the two carrier charge distributions each with itself. We do this by including only the Coulomb interaction between q_i^h and q_j^e. The desired electrostatic energy is therefore given by

$$E_C^{hc} + E_P + E_{CP} = \Delta\langle V \rangle_{ex} - \left(1 - \frac{1}{\varepsilon_r}\right) E_C \tag{12}$$

where E_C^{hc}, E_P and E_{CP} are sums of: interactions between q_i^c and q_i^h, polarization-polarization interactions, and charge-polarization interactions. We have replaced E_C^{hc} with $\Delta\langle V \rangle_{ex}$, and used $E_P + E_{CP} = -(1 - 1/\varepsilon_r)E_C$, where E_C is the sum of interactions between q_i and q_j. We replace the left-hand side of Equation 12 with U_{el} and sum over the whole chain to finally obtain

$$U_{el} = -\sum_{i,j} |a_i^h|^2 |a_j^e|^2 E_C^{hc}(i,j) - V_C \sum_i |a_i^h|^2 |a_i^e|^2$$

$$- \left(1 - \frac{1}{\varepsilon_r}\right) \frac{1}{2} \sum_{i,j} \left(|a_i^h|^2 - |a_i^e|^2\right)\left(|a_j^h|^2 - |a_j^e|^2\right) E_C(i,j) \tag{13}$$

The first two terms represent the hole-electron Coulomb interaction $\Delta\langle V \rangle_{ex}$, and the last term is the polarization energy, which we denote $\Delta\langle H_{pol} \rangle$. The factor $1/2$ in this term is used to avoid double-counting. $E_C(i,j)$ is the Coulomb integral of two smeared charge distributions located at i and j, described in detail in Ref [57] and summarized in Supplementary Information.

Reorganization energy of nuclei

The last term of the exciton energy is the stabilization of the hole-electron pair by the reorganization of nuclei. A detailed deriva-

tion of the reorganization energy for a charge carrier distributed over multiple sites can be found in our previous work[57]. More briefly here, the energy terms of the Hamiltonian involving the amplitude of distortion of the nuclei in response to a single carrier are

$$\langle H_{nuc} \rangle = U_0 \sum_i |a_i|^2 X_i + \frac{1}{2} U_0 \sum_i X_i^2 \quad (14)$$

Here X_i is the amplitude of distortion along a composite mode, i.e., the actual distortion of the nuclear coordinates in response to the presence of the carrier. X_i is normalized such that $X_i = -|a_i|^2$ at equilibrium. At this condition, $\langle H_{nuc} \rangle$ reduces to $-\frac{1}{2} U_0 \sum_i |a_i|^4$, where the constant U_0 characterizes the strength of interaction between a charge and the nuclei distortion it induces. We have shown in our previous work[57] that this constant is the same for both extra electrons and holes in P3HT, with a value of 0.66 eV.

For an extra electron and a hole simultaneously present on the same chain, the reorganization energy will be the sum of the two contributions to the distortion of the nuclei:

$$\Delta\langle H_{nuc} \rangle = -\frac{1}{2} U_0 \sum_i \left(|a_i^e|^4 + |a_i^h|^4 \right) \quad (15)$$

We verified the validity of this approach by comparing the prediction of Equation 15 to the relaxation energy of the singlet excited state for a single thiophene ring, for which the largest nuclear relaxation is expected. A difference of less than 0.1 eV is observed.

Exciton energy assembled

We assemble the kinetic energy of the hole and electron $\Delta\langle T \rangle$, the hole-electron Coulomb interaction $\Delta\langle V \rangle_e$, the polarization energy of the surrounding dielectric $\Delta\langle H_{pol} \rangle$, and the reorganization energy of the nuclei $\Delta\langle H_{nuc} \rangle$, to finally obtain the exciton energy with respect to the the hole and electron extended states $E_B^0 = \Delta\langle T \rangle + \Delta\langle V \rangle_{ex} + \Delta\langle H_{pol} \rangle + \Delta\langle H_{nuc} \rangle$, as follows:

$$\Delta E_B^0 = t_e \sum_i |a_{i+1}^e - a_i^e|^2 + |t_h| \sum_i |a_{i+1}^h - a_i^h|^2$$

$$- \sum_{i,j} |a_i^h|^2 |a_j^e|^2 E_C(i,j) + V_C \sum_i |a_i^h|^2 |a_i^e|^2$$

$$- \left(1 - \frac{1}{\varepsilon_r} \right) \frac{1}{2} \sum_{i,j} \left(|a_i^h|^2 - |a_i^e|^2 \right) \left(|a_j^h|^2 - |a_j^e|^2 \right) E_C(i,j)$$

$$- \frac{1}{2} U_0 \sum_i \left(|a_i^e|^4 + |a_i^h|^4 \right) \quad (16)$$

where i and j are site counters along the polymer chain.

Below, we use this expression to determine the optimal exciton configuration, including the width of the electron and hole probability densities and the binding energy, for an exciton on an isolated chain and on a chain in a polarizable medium. Unless otherwise noted the parameters used in computing E_B^0 are: $t_e = 0.76$ and $t_h = -0.98$ eV[58], $E_0 = 0.66$ eV[57], $V_C = 1.9$ eV, $\sigma = 2$ Å (see Eq S1), and $\varepsilon_r = 2$.

Optimal exciton configuration

To obtain the optimal configuration of the exciton, we minimize Eq (16) with respect to the electron and hole wavefunctions. We do this by imposing two variational wavefunctions, one for the hole and the other for the electron, and minimize the exciton energy with respect to their parameters. For convenience, we initially assume both electron and hole wavefunctions are represented by a Gaussian distribution across the chain. The amplitudes $\{a_i\}$ are given by

$$a_i = \frac{e^{-(i-i_0)^2/2\sigma^2}}{\left(\sum_i e^{-(i-i_0)^2/\sigma^2} \right)^{1/2}} \quad (17)$$

where σ and i_0 are the width and center of the Gaussian respectively. The optimal exciton configuration and associated energy is attained by minimizing E_B^0 with respect to the four parameters: i_0 and σ for the hole and electron wavefunctions. We will later relax the Gaussian constraint on the carrier envelope, when discussing exciton polarization and dissociation. This will be done by minimizing E_B^0 with respect to the whole set of site amplitudes $\{a_i\}$.
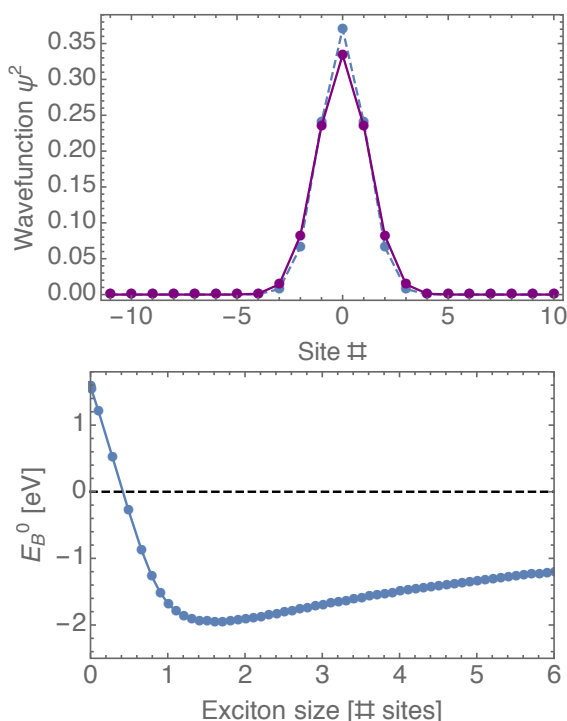
Exciton on isolated chain with no nuclei reorganization

We first consider the simple case of a singlet exciton formed by vertical excitation on an isolated P3HT chain. With no dielectric to polarize and no nuclear rearrangement, the terms $\Delta\langle H_{pol} \rangle$ and $\Delta\langle H_{nuc} \rangle$ of E_B^0 vanish. In this situation, the most stable singlet exciton has an electron and hole with coinciding charge centers, as shown in Figure 3a. Figure 3b displays the exciton binding energy versus exciton width. The exciton configuration is optimal at 1.6 rings or 6.4 Å, in good agreement with the results of Mewes et al.[65], who predicted a value of 7 Å for a number conjugated polymers by first-principle calculations at the Configuration Interaction Singles (CIS) level. The optimal exciton is -3.53 eV more stable than the exciton confined to a single site, and -1.95 eV more stable than the fully delocalized exciton, i.e., the hole and electron extended states in an infinitely long chain. The binding energy and exciton size for this configuration of the exciton are summarized in Table 1. The exciton size is here defined as $(\langle |r_e - r_h|^2 \rangle)^{1/2}$ or $\sum_{ij} |a_i^e|^2 |a_j^h|^2 R_{ij}^2$, where r_e and r_h are the electron and hole coordinates, respectively[65,66]. E_B^0 and E_B are iden-

Table 1 Binding energy and size of exciton on P3HT chain.

Medium	E_B^0 (eV)	E_B (eV)	Size (site)
Vaccum, no relaxation	1.95	1.95	1.6
Polarizable, with relaxation	2.13	0.95	1.5

tical in this case because of the absence of any polaronic effects (see Figure 1). The obtained binding energy is in good agreement with the GW-BSE prediction of van der Host et al[12] (1.85 eV), and our own TD-DFT calculations with LC-ωPBE* (1.91 eV), shown in Figure 2.

Fig. 3 (a) Optimal exciton configuration on an isolated P3HT chain, with no nuclei rearrangement. The exciton is 1.6 ring wide (see definition in text.) (b) Exciton binding energy with respect to hole and electron extented states (E_B^0) as a function of exciton size. The dashed line represents the asymptotic large-size limit.

Exciton on chain in a dielectric medium

Now we consider an exciton on a chain in a polarizable medium, and allow the nuclei to reorganize in response to the exciton. The terms of the exciton binding energy that control these effects, $\Delta\langle H_{pol}\rangle$ and $\Delta\langle H_{nuc}\rangle$, are now turned on. We adopt an effective dielectric constant $\varepsilon_r = 2$ for the polarizable medium surrounding the exciton. This dielectric constant reflects only the electronic contribution to the polarizability of P3HT, as discussed in detail in our previous work[57]. When $i = j$, we reduce this constant to 1.75, so that the local self-interaction in $\Delta\langle H_{pol}\rangle$ is less screened. This was done in order to match the polaronic stabilization to experiment for P3HT chains in the amorphous phase[67,68]. The total polaron stabilization energy of the two carriers sets the difference between E_B^0 and E_B, i.e., the exciton binding energy with respect the separated hole and electron polarons (See Figure 1.) E_B is the relevant binding energy for photocurrent generation and electroluminescence, and is therefore more practically meaningful.

Similar to the isolated chain, the optimized exciton is unpolarized, with its hole and electron center of charges co-located along the chain. The binding energies and exciton size are listed in Table 1. The binding energy with respect to the two carriers extended states E_B^0 differs from that of the isolated chain by -0.18 eV, solely due to the nuclei reorganization energy. This effect also accounts for the small decrease in exciton size. Polarization has no stabilizing effect on the exciton, because the optimal co-location of the two carriers ensures a perfectly neutral quasiparticle. The exciton binding energy E_B with respect to the polaron

state of two separated carriers is about 1 eV lower than for the isolated chain, because of polaronic effects arising mainly from polarization. Such reduction in binding energy, when going from an isolated chain to a chain in a dielectric, was also reported by Sun *et al.*[9] (1.93 to 0.97 eV) who used non-empirically tuned range-corrected TD-DFT, and by van der Horst *et al*[12] (1.85 to 0.76 eV) using the GW-BSE approach. The agreement between this work and these more rigorous approaches is both qualitative and quantitative. Our prediction of the exciton binding energy with respect to the free hole and electron polaron, $E_B = 0.9$ eV, is also close to the experimental value of 0.7 eV determined by careful measurements of the transport and optical gaps[8,69] (see Figure 1).

Now that we have the value of E_B, we can map out the potential energy surface between the bound exciton and the separated polarons. The potential will also be useful to understand how the exciton is unbound by external forces, such as an applied electric field and a donor-acceptor interface.

Exciton dissociation potential

We next map out the exciton binding potential, i.e., the binding energy E_B^0 as a function of distance between the hole and the electron. The same variational approach outlined above is followed, but with the constraint of a fixed distance between the centre of charges of the two carriers. We control the separation distance by fixing the parameter i_0 for the two trial wavefunctions, and minimize E_B^0 with respect to σ for the two envelopes. The exciton potential for parameters corresponding to P3HT is given in Figure 4.
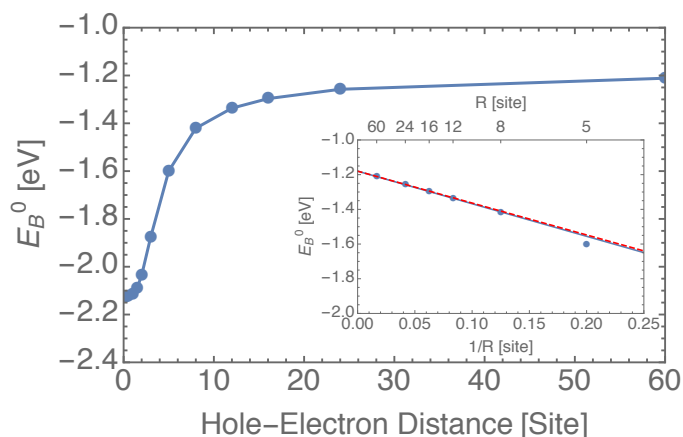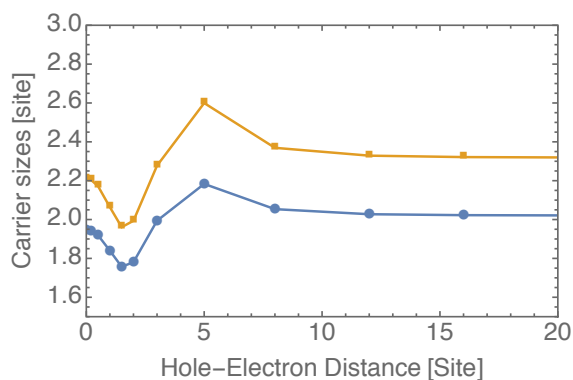

Fig. 4 Exciton potential, i.e., binding energy as a function of hole-electron distance, for P3HT obtained with $\varepsilon_r = 2.0$. (Inset) Extrapolation to infinite separation. Energy is plotted versus $1/R$ (R the hole-electron distance). Solid line is a fit to first four points; while dashed line is a pure Coulomb interaction with the same intercept.

The potential follows the expected Coulomb behavior of two interacting bare charges at large separation, as shown in inset of Figure 4. At small separations, the spreading of the charge distributions leads to deviation from this behavior. E_B can be clearly understood from the two Figures, 4 and inset, as the difference between the minimum in the binding potential, which occurs at

zero separation distance, and the value of the potential at the large separation limit, where E_B^0 approaches the value for isolated hole and electron polarons.

We also observe the size of the hole and electron probability distributions at various separation distances along the exciton potential (See Figure 5.) The size is measured as twice the standard

Fig. 5 Evolution of the hole and electron sizes as the two carriers approach each other.

Fig. 6 (a) Exciton potential for different dielectric constants ε_r. The value used are (top to bottom curve): $\varepsilon_r = 2$, $\varepsilon_r = 3$, $\varepsilon_r = 5$, $\varepsilon_r = 10$, $\varepsilon_r = 20$, and $\varepsilon_r = \infty$. (b) Exciton binding energy with respect to polaron states as a function of dielectric constant (data points.) The dashed line represents c/ε_r.

deviation of the probability density. Far away from each other the two carriers have a size determined by polarization and ring reorganization. The charge carriers maintain these sizes as their separation distance decreases until their charge distributions begin to overlap. At this point, the carriers compete to polarize the same medium. This competition contributes a positive energy to their interaction, and the carriers expand to minimize this effect. When brought even closer, the two carriers begin to shrink in order to maximize the attractive Coulomb interaction between them. At very short separation distances, two sites and below, the competition to polarize the same medium dominates the interaction between the two carriers; they expand to minimize the repulsive contribution to their interaction (see binding potential at higher ε_r in Figure 6a).

All results above have used a dielectric constant $\varepsilon_r = 2$. We now consider how the binding potential is affected by the magnitude of ε_r.

Effect of dielectric constant on exciton binding potential

The dielectric constant of the medium affects the stability of the separated electron and hole polarons, and controls the screening of their Coulomb interaction. A more polarizable medium leads to more stable hole and electron polarons, and more effective screening of the Coulomb interaction between the separated carriers. The result is a reduced binding energy of the exciton relative to the polaron states E_B (See Figure 6.)

Figure 6a reveals that the Coulomb attraction between the carriers at zero separation distance is unchanged, regardless the dielectric constant, because the corresponding exciton is everywhere uncharged. The polaron stability as well as the path from bound exciton to polarons is strongly affected by the dielectric constant. For a dielectric constant of $\varepsilon_r = 3$ and larger, the strongly screened Coulomb attraction is overcome by the the short-range repulsive competition to polarize the dielectric, such
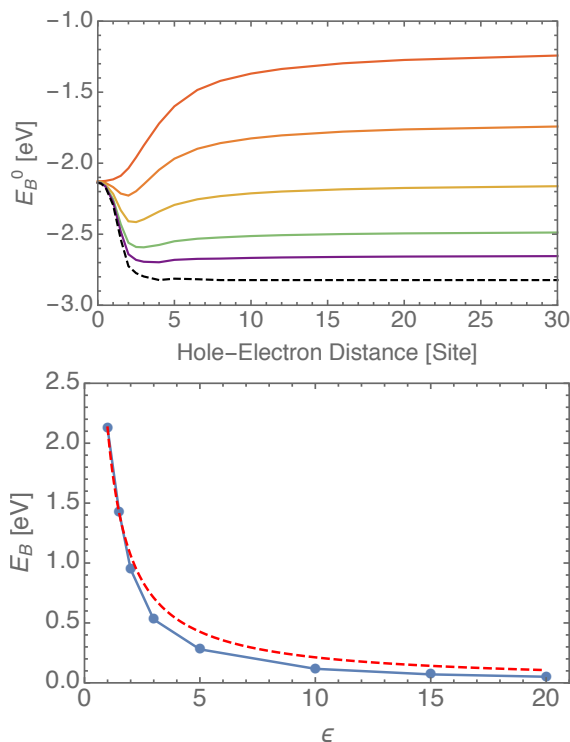
that the exciton becomes more stable when the carriers sit some short distance apart (see the position of the binding potential minimum.) This picture is analogous to a solvent-separated ion pair, for which the optimal configuration involves two ions separated by some short distance. The formation and stability of such ion pairs is primarily dictated by the dielectric constant of the solvent.

We also see that the depth of the minimum in the binding potential decreases with increasing dielectric constant ε_r. Figure 6b shows the exciton binding energy as a function of dielectric constant. The behavior of E_B versus ε_r closely follows the c/ε_r trend expected of two interacting point charges in a dielectric medium, as shown by the dashed curve. The constant c was adjusted to match E_B for $\varepsilon_r = 1$. The deviation observed at intermediate dielectric constant is due to the solvent-separated-pair effect explained above.

At very large dielectric constant, the binding energy can fall below the threshold of thermal energy at ambient temperature (kT), and the exciton would readily dissociate after formation. Given the hopping parameters of P3HT, the relative permittivity for which E_B would match kT is $\varepsilon_r = 40$. Increasing the dielectric constant of the photoactive layer is being pursued as an avenue for increasing the exciton separation efficiency and therefore the power conversion efficiency of organic photovoltaics[70]. As potentially effective as this strategy may be, one must keep in mind that a high dielectric constant also leads to more stable polaron states[57], with associated reduced carrier mobility[71]. One must also consider the polarization mechanism, not just the magnitude

of the dielectric constant, since slow polarization modes may not be effective at screening the hole-electron Coulomb interaction.

Exciton polarization and dissociation

Unconstrained exciton wavefunctions

Before examining the dissociation of the exciton in an electric field and at a donor-acceptor 1D interface, we introduce the following simplification: we set t_e and t_h to 0.98 eV, the hopping integral of the hole. This decouples the effects of the introduced external factors on the probability distribution of carriers from those associated with the difference of hopping integrals. We also relax the constraint that restricts the shape of the hole and electron envelopes to a Gaussian, so that we have no restriction on the shape the individual carrier wavefunctions can adopt. In other words, we minimize the binding energy E_B^0, given by Equation 16, with respect to the entire set of wavefunction onsite amplitudes $\{a_i\}$.

We find that the optimal states deviate from a Gaussian shape, as external factors (electric field and interface) are added to polarize the charge carrier distributions. As above, the binding potential is obtained by performing the minimization for different separation distances between hole and electron. We use umbrella potentials to control the positions of the two centers of charge. The resulting potential is portrayed in Figure 7a. We have used
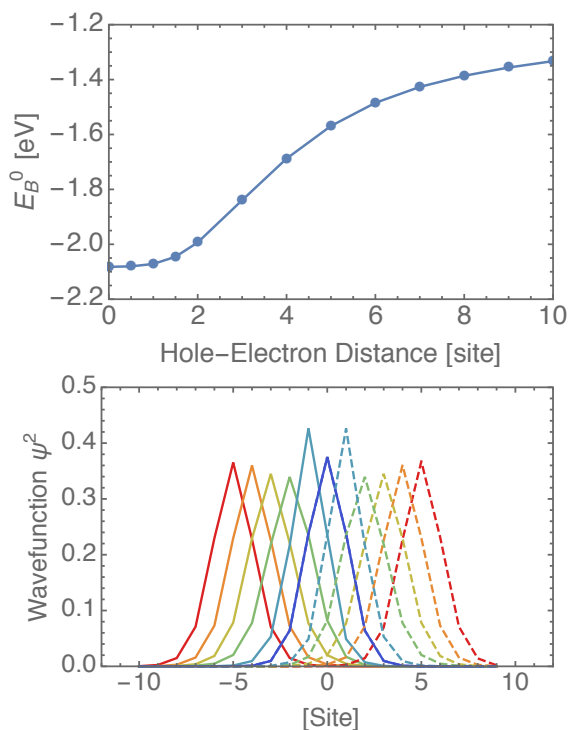

Fig. 7 (a) Exciton potential without Gaussian constraint, for P3HT obtained with $\varepsilon_r = 2.0$. (b) Wave functions involved in the exciton potential in (a); the dashed curves are for the hole, and the solid curves for the electron.

a smaller system size (20 sites) because of the larger cost of minimizing over the whole set of $\{a_i\}$. Examples of the resulting charge carrier probability distributions are shown in Figure 7b, where the solid line is for the electron, and the dashed line for

the hole. The distributions are color-coded by their relative distance.

Exciton in an electric field

We examine the exciton binding potential under an applied external electric field. The external electric field applied along the direction of the chain adds a linear potential of the form $U = -Ez$, where E is the field and z is the coordinate along the chain axis. It introduces a bias for pulling the charge carriers apart, i.e., the energy decreases when the electron moves down the field and the hole moves up the field. The result is a tilted binding potential, as shown in Figure 8.
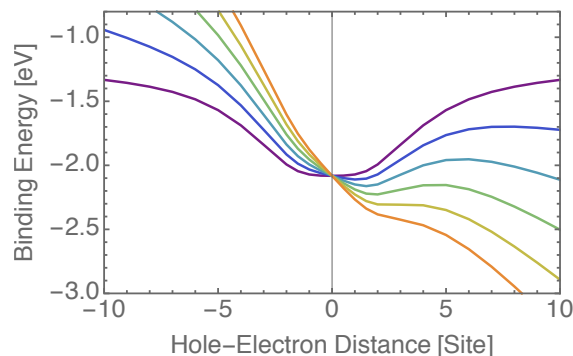
Fig. 8 Effect of applied external electric field of various strengths on the exciton. The field strengths are $E = \{0.0, 0.01, 0.02, 0.03, 0.04, 0.05\}$ from the top curve to the bottom one, respectively.

Figure 8 was obtained by adding to the bare exciton potential (see Figure 7a,) a linear potential U with magnitudes of E ranging between 0 and 0.05 V/Å. The figure reveals that the field reduces the depth of the binding/dissociation potential minimum; larger field strengths lead to a shallower minimum. The field that just manages to suppress the minimum in the potential is able to unbind the charge carriers. The value of this threshold field is 39 mV/Å; however, exciton dissociation can practically occur when the depth of the minimum is comparable to kT. Negative values of the x-axis in Figure 8 indicate separations of an electron and hole in a direction that opposes the electric field.

The threshold field is equal to the largest attractive force between the electron and hole. This force corresponds to the largest slope in the exciton binding potential. Figure S2 shows the slope of the bare binding potential (see Figure 7a) as a function of the hole-electron distance. The maximum force of attraction between the two carriers is around 40 meV/Å, which matches the field strength that leads to dissociation in Figure 8.
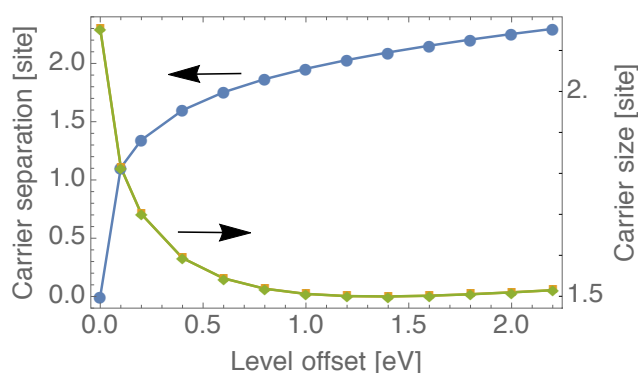
We have seen that, without the contribution of other factors to aid the exciton dissociation, a large external electric field is required to overcome the Coulomb attraction between the hole and the electron. In practice, organic photovoltaics rely on the presence of two semiconducting materials for efficient photocurrent generation. An electron donor material, in which excitons usually form by photo-excitation, is mixed with an electron acceptor, such that the HOMO/LUMO energy level offset at the interface between the two materials facilitates the dissociation of excitons.

Below we examine quantitatively the role played by such interface in the generation of free charge carriers.

Covalent donor-acceptor interface

Here we look at an exciton at an idealized covalent interface between donor and acceptor blocks, with a HOMO energy difference Δ_{D-A} (level offset) between the two polymer segments. For simplicity we assume both the HOMO and the LUMO on one side of the interface are shifted by the same amount. This is done by adjusting the onsite energy parameters (Equation 1) across the interface. We place the interface exactly between the two middle sites along the chain, and leave the hopping parameters unmodified between all sites.
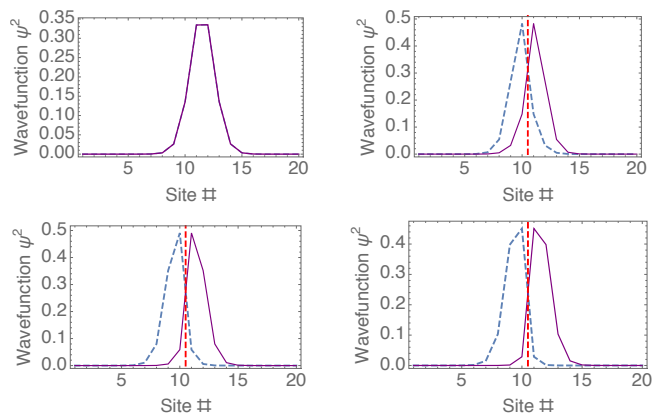
The effects of the energy level offset at the interface are shown in Figure 9, where the distance between the center of charge of the electron and the hole is plotted versus the level offset. The exciton is increasingly polarized at the interface as the

Fig. 10 Hole and electron wavefunctions for four different values of the HOMO level offset at the interface. The values of the offset are {0.0, 0.2, 1.0, 2.0} eV.

Fig. 9 Effect of the HOMO level offset on the exciton. The hole-electron distance evolves with the magnitude of the offset (primary y-axis). Evolution of the carrier sizes with HOMO level offset or hole-electron distance (secondary y-axis).

HOMO/LUMO energy level offset increases. Once the offset is large enough to achieve a separation of one unit, the slope of Figure 9 decreases with carrier sizes, to maximize their Coulomb interaction. Increasing the energy offset at the interface is an effective strategy for overcoming this attraction only up to a certain magnitude, beyond which the benefit of this strategy becomes marginal. This is important to realize for the optimization of organic solar cells, where there is a trade-off between the energy level offset driving exciton dissociation and the device open circuit voltage.

The dissociation of the exciton is accompanied by a change in shape and size of the charge carriers. The size versus offset is also plotted in Figure 9 (see secondary y-axis), which reveals that the electron and hole shrink when they are pulled apart by the interface. (Here the size change is the same for the two carriers, because we assumed they have the same hopping matrix elements.) The hole and electron shape adjustment is evident from Figure 10, where representative carrier probability distributions are shown. The carrier wavefunctions became asymmetric to keep the two centers of charge close to each other while stay-

ing on the favored side of the interface. The hole favors the side of the interface with a higher HOMO, while the electron prefers the side with a lower LUMO. As a result, the exciton shows a preference for being at the interface whenever an energy level offset exists.

To better understand the effect of the interface on the exciton, we show how the level offset affects the exciton binding potential. Figure 11 displays the potential for three different scenarios: (1) in the absence of any HOMO/LUMO offset, and (2) and (3) when an energy offset of 0.2 and 0.3 eV exists at the interface, respectively. It is energetically less expensive to pull the exciton
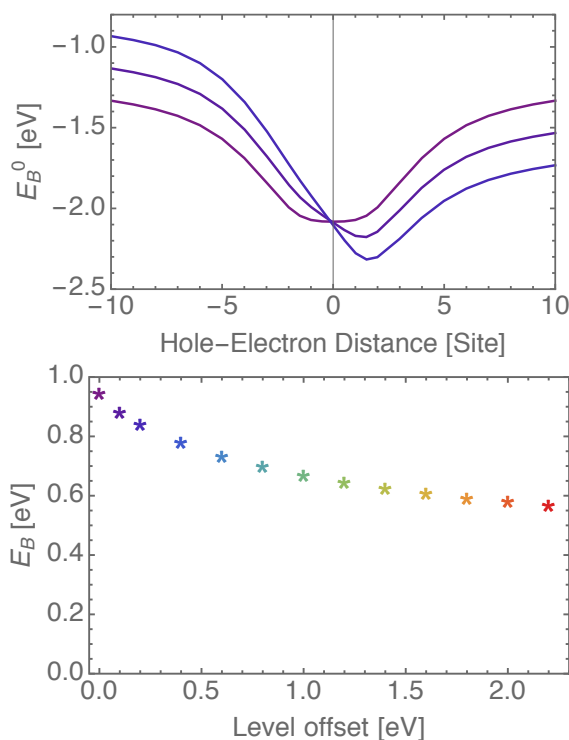

Fig. 11 (a) Effect of the level offset on the exciton potential. The values of the offset are 0.0, 0.2 and 0.4 eV. (b) Binding energy with respect to separated polarons versus level offset.

apart when the hole is on the higher-HOMO side of the interface and the electron is on the lower-LUMO side of the interface (positive distances in Figure 11). This bias is reflected in tilted binding potentials when there is a level offset (non-symmetric curves) compared to the situation with no level offset (symmetric curve).

We observe a reduction in binding energy with respect to the separated polarons E_B, but the reduction does not increase linearly with the level offset (See Figure 11b). This is because both the separated polaron state (see potential at infinity) and the minimum in the binding potential shift down to lower energies with the level offset. However, the energy change for the polaron state matches exactly the level offset, whereas the change in the binding potential minimum does not. The minimum shifts from the optimal singlet exciton, in the absence of any level offset, to a configuration in which the electron and hole centers of charge respectively lie on the acceptor and and the donor side of the interface (see also Figure 10), called the charge transfer (CT) state. A possible strategy for further improving the rate of exciton dissociation in organic solar cells could be by raising the energy of the CT state relative to the optimal singlet exciton, for a given level offset.

We have seen that the donor-acceptor interfacial energy level offset weakens the hole-electron interaction by producing CT states with a reduced binding energy E_B relative to the singlet exciton in the donor material. The CT state is easier to unbind. To illustrate that, we determine the critical field that unbinds the exction for different magnitudes of the offset. We summarize the critical field as a function of the energy level offset in Figure 12. As anticipated from the binding energy versus level offset trend
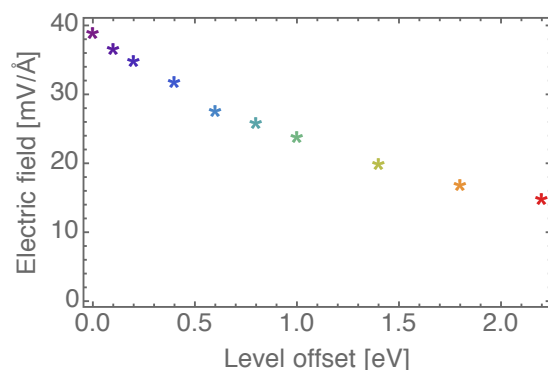
Fig. 12 Required field for dissociation (of the CT state) as a function of the level offset at the D-A interface.

discussed above (See Figure 11b), Figure 12 shows the field required to unbind the CT state decreases with the level offset. This can also be seen from the tilted binding potentials in Figure 11a. These potentials have a reduced maximum slope (attractive force between the two charge carriers) in the second half of the figure, so that a smaller field is required to overcome the hole-electron attraction. However, even with an offset as large as 2 eV, a still large field of 15 mV/Å is needed for complete dissociation.

CT state binding energy are routinely estimated based on the interfacial intermolecular distance and even measured to be about 0.5 eV[72,73], but a value as high as 0.84 eV has been re-

ported for molecular organic semiconductors[74]. Given the high internal quantum efficiency of some high-performing organic photovoltaic devices, many explanations for how the hole and electron escape the still-large Coulomb binding energy of the CT state have been suggested. One such explanation is that the excess energy available after dissociation of the bound exciton at the interface leads to the formation of a 'hot CT state', as opposed to the lowest-energy CT state, with more delocalized electron and hole, and easier to unbind[75,76]. Another explanation suggests that the generation of free carriers from the CT state is aided by energetic disorder and dynamic effects[59,60,77]. We did not consider disorder in this work, though our flexible and cost effective tight-binding model can lend itself well to the study of the effects of both energetic and spatial disorder at the interface on the dissociation of the CT state.

Conclusions

We have developed a model based on the tight binding approximation for the description of singlet excitons on one-dimensional polythiophene chains. Our model is similar in some respects to the Pariser-Parr-Pople model, but we treat the electron and hole and the their effective interaction explicitly, which allows for a simultaneous description of the two carriers spatial probability distribution. Our model also takes into account the carrier-induced reorganization of nuclei along the chain and the polarization of the surrounding dielectric medium. These effects are responsible for the formation of polarons when the hole and electron are separated, and for screening the interaction between the two particles, in the case of dielectric polarization.

We used this model to study the binding and dissociation of excitons on single chains. On an isolated P3HT chain, we find that vertical excitons have a binding energy of about 1.9 eV. When we turn on reorganization of nuclei and consider a chain in a polarizable medium, we observe that nuclear reorganization lowers the exciton energy by about 0.2 eV, but the binding energy is reduced to 0.9 eV because of polaronic effects arising mainly from dielectric polarization. These findings agree well with higher level calculations following the GW-BSE approach and TD-DFT with tuned range-corrected hybrid functionals.

We computed the exciton binding potential, and study the effect of the dielectric constant of the surrounding medium. We define the exciton binding energy as the energy difference between the minimum in the potential and its value at infinite charge separation, which corresponds to two separated polarons. Polarization, governed by the dielectric constant, dictates the value of the potential at infinity and screens the hole-electron interaction. For dielectric constant larger than 2, the optimal exciton adopts a configuration resembling a solvent-separated ion pair, in which the hole and electron center of charges are separated by some distance. The binding energy closely follows an inverse relationship with the dielectric constant, with a small deviation for intermediate dielectric constants due to the solvent-separated-pair effect.

We then investigated the effects on the exciton of an applied electric field and a covalent donor-acceptor interface . We find that the field tilts the exciton binding potential. The critical field to unbind the exciton is the field that just manages to suppress the

minimum in the potential. This field equals the maximum attractive force between the hole and electron, i.e., the largest slope in the binding potential. We also show how a donor-acceptor interface with a given HOMO/LUMO energy offset pulls the hole and electron apart, and forms a charge-transfer state with reduced binding energy. The binding energy decreases with increasing level offset, but the effect quickly saturates at high offset values. Along with a reduction in binding energy, the level offset also reduces the maximum slope in the hole-electron binding potential, such that the hole-electron pair can be more easily unbound.

As demonstrated in this work for P3HT, our transparent tight binding model offers the potential to answer a number of pertinent questions on the properties and behavior of exciton in conjugated polymers as relevant for photovoltaics. While we have not shown and cannot claim that our method will work for all conjugated polymers, we have no reason to doubt its applicability to other conjugated polymers to some extent. The parameters that enter the model, namely the hole and electron hopping integrals, the effective onsite interaction parameter, the characteristic nuclear reorganization energy, the effective dielectric constant and the size of the moiety constituting a site, can all be determined for other conjugated polymers. Efforts along this direction are underway, including the application of the model to push-pull copolymers, and will be the subject of a future publication.

Acknowledgements

Conflict of interest

There are no conflicts of interest to declare.

References

1 J. H. Burroughes, D. D. C. Bradley, a. R. Brown, R. N. Marks, K. Mackay, R. H. Friend, P. L. Burns and a. B. Holmes, *Nature*, 1990, **347**, 539–541.

2 F. Garnier, R. Hajlaoui, A. Yassar and P. Srivastava, *Science*, 1994, **265**, 1684–1686.

3 N. Sariciftci, L. Smilowitz, a.J. Heeger and F. Wudl, *Synthetic Metals*, 1993, **59**, 333–352.

4 J. Brebels, J. V. Manca, L. Lutsen, D. Vanderzande and W. Maes, *Journal of Materials Chemistry A*, 2017, **5**, 24037–24050.

5 H. Kang, G. Kim, J. Kim, S. Kwon, H. Kim and K. Lee, *Advanced Materials*, 2016, **28**, 7821–7861.

6 K. A. Mazzio and C. K. Luscombe, *Chemical Society Reviews*, 2015, **44**, 78–90.

7 C. Deibel and V. Dyakonov, *Reports on Progress in Physics*, 2010, **73**, 096401.

8 C. Deibel, D. Mack, J. Gorenflot, A. Schöll, S. Krause, F. Reinert, D. Rauh and V. Dyakonov, *Physical Review B*, 2010, **81**, 085202.

9 H. Sun, Z. Hu, C. Zhong, S. Zhang and Z. Sun, *The Journal of Physical Chemistry C*, 2016, **120**, 8048–8055.

10 J.-L. Bredas, *Mater. Horiz.*, 2014, **1**, 17–19.

11 J.-W. van der Horst, P. A. Bobbert, M. A. J. Michels, G. Brocks and P. J. Kelly, *Physical Review Letters*, 1999, **83**, 4413–4416.

12 J.-W. van der Horst, P. A. Bobbert, P. H. L. de Jong, M. A. J. Michels, G. Brocks and P. J. Kelly, *Physical Review B*, 2000, **61**, 15817–15826.

13 J. W. Van Der Horst, P. A. Bobbert, M. A. J. Michels and H. Bässler, *Journal of Chemical Physics*, 2001, **114**, 6950–6957.

14 J.-W. van der Horst, P. Bobbert, W. Pasveer, M. Michels, G. Brocks and P. Kelly, *Computer Physics Communications*, 2002, **147**, 331–334.

15 J.-W. van der Horst, P. Bobbert and M. Michels, *Synthetic Metals*, 2003, **135-136**, 281–282.

16 G. Samsonidze, F. J. Ribeiro, M. L. Cohen and S. G. Louie, *Physical Review B*, 2014, **90**, 035123.

17 M. Rohlfing and S. G. Louie, *Physical Review B*, 2000, **62**, 4927–4944.

18 M. Rohlfing and S. G. Louie, *Physical Review Letters*, 1999, **82**, 1959–1962.

19 D. Jacquemin, I. Duchemin and X. Blase, *Journal of Chemical Theory and Computation*, 2015, **11**, 3290–3304.

20 M. L. Tiago, M. Rohlfing and S. G. Louie, *Physical Review B*, 2004, **70**, 193204.

21 M. L. Tiago, J. E. Northrup and S. G. Louie, *Physical Review B*, 2003, **67**, 115212.

22 X. Wang, T. Garcia, S. Monaco, B. Schatschneider and N. Marom, *CrystEngComm*, 2016, **18**, 7353–7362.

23 N. Sai, M. L. Tiago, J. R. Chelikowsky and F. A. Reboredo, *Physical Review B*, 2008, **77**, 161306.

24 I. Duchemin and X. Blase, *Physical Review B*, 2013, **87**, 245412.

25 F. Bruneval, S. M. Hamed and J. B. Neaton, *The Journal of Chemical Physics*, 2015, **142**, 244101.

26 X. Blase, I. Duchemin and D. Jacquemin, *Chemical Society Reviews*, 2018, **47**, 1022–1043.

27 J. P. Perdew, K. Burke and M. Ernzerhof, *Physical Review Letters*, 1996, **77**, 3865–3868.

28 C. Lee, W. Yang and R. G. Parr, *Physical Review B*, 1988, **37**, 785–789.

29 A. D. Becke, *The Journal of Chemical Physics*, 1993, **98**, 5648–5652.

30 P. J. Stephens, F. J. Devlin, C. F. Chabalowski and M. J. Frisch, *The Journal of Physical Chemistry*, 1994, **98**, 11623–11627.

31 T. Stein, L. Kronik and R. Baer, *Journal of the American Chemical Society*, 2009, **131**, 2818–2820.

32 J. Autschbach and M. Srebro, *Accounts of Chemical Research*, 2014, **47**, 2592–2602.

33 T. Körzdörfer and J.-L. Brédas, *Accounts of Chemical Research*, 2014, **47**, 3284–3291.

34 A. Ruzsinszky, J. P. Perdew, G. I. Csonka, O. A. Vydrov and G. E. Scuseria, *The Journal of Chemical Physics*, 2006, **125**,

194112.

35 P. Mori-Sánchez, A. J. Cohen and W. Yang, *The Journal of Chemical Physics*, 2006, **125**, 201102.

36 S. Kümmel and L. Kronik, *Reviews of Modern Physics*, 2008, **80**, 3–60.

37 A. J. Cohen, P. Mori-Sánchez and W. Yang, *Chemical Reviews*, 2012, **112**, 289–320.

38 H. Iikura, T. Tsuneda, T. Yanai and K. Hirao, *The Journal of Chemical Physics*, 2001, **115**, 3540–3544.

39 O. A. Vydrov and G. E. Scuseria, *The Journal of Chemical Physics*, 2006, **125**, 234109.

40 J.-D. Chai and M. Head-Gordon, *The Journal of Chemical Physics*, 2008, **128**, 084106.

41 R. Baer, E. Livshits and U. Salzner, *Annual Review of Physical Chemistry*, 2010, **61**, 85–109.

42 S. Refaely-Abramson, S. Sharifzadeh, N. Govind, J. Autschbach, J. B. Neaton, R. Baer and L. Kronik, *Physical Review Letters*, 2012, **109**, 226405.

43 H. Tamura and I. Burghardt, *The Journal of Physical Chemistry C*, 2013, **117**, 15020–15025.

44 S. Refaely-Abramson, M. Jain, S. Sharifzadeh, J. B. Neaton and L. Kronik, *Physical Review B*, 2015, **92**, 081204.

45 G. Heimel, *ACS Central Science*, 2016, **2**, 309–315.

46 Y. Zhang, R. Steyrleuthner and J.-L. Bredas, *The Journal of Physical Chemistry C*, 2016, **120**, 9671–9677.

47 W. P. Su, J. R. Schrieffer and A. J. Heeger, *Physical Review Letters*, 1979, **42**, 1698–1701.

48 W. P. Su, J. R. Schrieffer and A. J. Heeger, *Physical Review B*, 1980, **22**, 2099–2111.

49 A. J. Heeger, S. Kivelson, J. R. Schrieffer and W. P. Su, *Reviews of Modern Physics*, 1988, **60**, 781–850.

50 Z. Shuai, J. L. Brédas, S. K. Pati and S. Ramasesha, *Physical Review B*, 1998, **58**, 15329–15332.

51 L. A. Ribeiro, W. F. da Cunha, P. H. Oliveira Neto, R. Gargano and G. M. e Silva, *Chemical Physics Letters*, 2013, **580**, 108–114.

52 J. Hubbard, *Proceedings of the Royal Society A: Mathematical, Physical and Engineering Sciences*, 1963, **276**, 238–257.

53 W. Barford and N. Paiboonvorachat, *The Journal of Chemical Physics*, 2008, **129**, 164716.

54 D. Zhang, Z. Qu, C. Liu and Y. Jiang, *The Journal of Chemical Physics*, 2011, **134**, 024114.

55 Z. Hu, A. P. Willard, R. J. Ono, C. W. Bielawski, P. J. Rossky and D. A. Vanden Bout, *Nature Communications*, 2015, **6**, 8246.

56 Z. Sun, S. Li, S. Xie and Z. An, *Organic Electronics*, 2018, **57**, 277–284.

57 J. H. Bombile, M. J. Janik and S. T. Milner, *Physical Chemistry Chemical Physics*, 2018, **20**, 317–331.

58 J. H. Bombile, M. J. Janik and S. T. Milner, *Phys. Chem. Chem. Phys.*, 2016, **18**, 12521–12533.

59 S. Barth, D. Hertel, Y.-H. Tak, H. Bässler and H. Hörhold, *Chemical Physics Letters*, 1997, **274**, 165–170.

60 S. N. Hood and I. Kassal, *The Journal of Physical Chemistry Letters*, 2016, **7**, 4495–4500.

61 Z. Sun and S. Stafström, *Physical Review B*, 2014, **90**, 115420.

62 K. Ohno, *Theoretica Chimica Acta*, 1964, **2**, 219–227.

63 H. Sun, C. Zhong and J.-L. Brédas, *Journal of Chemical Theory and Computation*, 2015, **11**, 3851–3858.

64 Y. Wang and J. P. Perdew, *Physical Review B*, 1991, **43**, 8911–8916.

65 S. A. Mewes, F. Plasser and A. Dreuw, *The Journal of Physical Chemistry Letters*, 2017, **8**, 1205–1210.

66 F. Plasser, B. Thomitzni, S. A. Bäppler, J. Wenzel, D. R. Rehn, M. Wormit and A. Dreuw, *Journal of Computational Chemistry*, 2015, **36**, 1609–1620.

67 R. Österbacka, *Science*, 2000, **287**, 839–842.

68 S. Kahmann, M. A. Loi and C. J. Brabec, *Journal of Materials Chemistry C*, 2018, **6**, 6008–6013.

69 H.-W. Li, Z. Guan, Y. Cheng, T. Lui, Q. Yang, C.-S. Lee, S. Chen and S.-W. Tsang, *Advanced Electronic Materials*, 2016, **2**, 1600200.

70 J. Brebels, J. V. Manca, L. Lutsen, D. Vanderzande and W. Maes, *Journal of Materials Chemistry A*, 2017, **5**, 24037–24050.

71 S. Y. Leblebici, T. L. Chen, P. Olalde-Velasco, W. Yang and B. Ma, *ACS Applied Materials & Interfaces*, 2013, **5**, 10105–10110.

72 X.-Y. Zhu, Q. Yang and M. Muntwiler, *Accounts of Chemical Research*, 2009, **42**, 1779–1787.

73 S. Tscheuschner, H. Bässler, K. Huber and A. Köhler, *The Journal of Physical Chemistry B*, 2015, **119**, 10359–10371.

74 N. R. Monahan, K. W. Williams, B. Kumar, C. Nuckolls and X.-Y. Zhu, *Physical Review Letters*, 2015, **114**, 247003.

75 A. A. Bakulin, A. Rao, V. G. Pavelyev, P. H. M. van Loosdrecht, M. S. Pshenichnikov, D. Niedzialek, J. Cornil, D. Beljonne and R. H. Friend, *Science*, 2012, **335**, 1340–1344.

76 G. Grancini, M. Maiuri, D. Fazzi, A. Petrozza, H.-J. Egelhaaf, D. Brida, G. Cerullo and G. Lanzani, *Nature Materials*, 2013, **12**, 29–33.

77 L. Shi, C. K. Lee and A. P. Willard, *ACS Central Science*, 2017, **3**, 1262–1270.